High pressure phase diagram of helium-hydrogen calculated through fluid integral equations and density functional theory of freezing

1991 J. Phys.: Condens. Matter 3 1613

(http://iopscience.iop.org/0953-8984/3/11/019)

J. Phys.: Condens. Matter 3 (1991) 1613–1625. Printed in the UK

High pressure phase diagram of helium–hydrogen calculated through fluid integral equations and density functional theory of freezing*

Willem L Vos†, André de Kuijper†, Jean-Louis Barrat‡ and Jan A Schouten†

† van der Waals laboratorium, Universiteit van Amsterdam, Valckenierstraat 67, 1018 XE Amsterdam, The Netherlands

‡ Ecole Normale Supérieure de Lyon, Laboratoire de Physique, 46, Allée d'Italie, 69364 Lyon Cédex 07, France

Received 7 November 1990, in final form 2 January 1991

Abstract. The HMSA integral equation has been solved for the binary mixture He–H_2 over a range of densities and compositions at 100 K and 300 K. Comparison of the radial distribution functions and the pressures shows that the results of the HMSA are in very good agreement with those of two-component MC simulations close to the binodal curve or the melting line. The HMSA equation of state, rather than the usual van der Waals one fluid approximation, was used to calculate the Gibbs free enthalpy; the latter was used to determine the fluid–fluid phase separation in the mixture. The agreement with experiments is reasonable. However, the spinodal curve, calculated from the composition fluctuation structure factor $S_{CC}(k)$, is not consistent with the binodal curve. This is probably due to inconsistencies in this structure factor. The direct correlation functions that result from the integral equations were used to calculate the freezing of the mixture with the Haymet and Oxtoby version of density functional theory of freezing, where the grand potential of the solid is expanded up to second order. To force quantitative agreement with experimental results, the fourth star was omitted from the HCP reciprocal lattice. An important result is the solubility of helium in the hydrogen-rich solid of a few mole percent. We also find the interesting phenomenon of density inversion between the hydrogen-rich solid and the hydrogen-rich fluid, as was observed experimentally. The results on the helium-rich side are inconsistent, probably because the truncation of the expansion of the grand potential of the solid after second order cannot handle the large difference in density and composition.

1. Introduction

The study of mixtures at high densities has received increasing interest in the past several years [1]. A theory used to describe succesfully fluid–fluid separation of binary mixtures is variational perturbation theory [2, 3] in conjunction with the van der Waals one fluid (VDW1F) approximation [4]. In variational perturbation theory, the free energy of the system is calculated with respect to a hard sphere reference system, where the hard sphere diameter is varied to obtain a minimal free energy. The VDW1F takes the properties of the mixture to be those of a single, hypothetical, pure fluid. The liquidus of the solid–fluid equilibria is also well described by the variational perturbation theory with VDW1F

* 410th publication of the van der Waals laboratorium.

0953-8984/91/111613 + 13 $03.50

in conjunction with an empirical freezing rule [3]. Variational and perturbation theories yield good thermodynamic data, but it is known that they do not yield correct structural data [5]. In those cases where good structural and thermodynamic data are required, integral equations are the appropriate tools. Furthermore, the VDW1F approximation breaks down for systems consisting of very dissimilar particles and becomes worse at high densities. Recently, there have been efforts to devise integral equations that are useful at high densities [6–8]. The results of these theories compare very well with computer simulation data [5], but they have not yet been tested on binary mixtures at very high density. Nevertheless, they seem promising for use under extreme conditions. Furthermore, it is interesting to calculate fluid–fluid phase separation of binary mixtures with these theories, since this has not yet been done.

A modern theory of the liquid–solid transition is the density functional theory of freezing [9] (DFTF); the basic idea of which is to describe the solid as an inhomogeneous fluid. It yields good results when compared to computer simulations for hard spheres (HS) [10]. It has also been applied to HS mixtures by Barrat *et al* [11] and Smithline and Haymet [12], adhesive hard spheres by Zheng and Oxtoby [13] and to Lennard–Jones (LJ) mixtures by Rick and Haymet [14]. However, the results for HS mixtures are in semiquantitative agreement with simulations [15]. In a recent paper [16], it was shown by us that none of the DFTF formulations yield good agreement with computer simulations using the LJ and Weeks, Chandler and Andersen (WCA)–reference–LJ potentials and experimental melting data of helium and hydrogen at high pressure. For pure helium and hydrogen, an empirical correction is applied to account for higher-order terms. It is worthwhile to test the usefulness of this DFTF version on the phase diagram of binary mixtures at high pressure, since it seems the only way to calculate both liquidus and solidus.

Among the binary mixtures studied at high pressure, He–H_2 stands out for its simplicity, which makes it suitable for theoretical description, and for its importance in astronomy, since it constitutes the interiors of the giant planets. He–H_2 has been investigated experimentally by Street [17] at pressures up to 10 kbar and by Loubeyre *et al* [18] and van den Bergh and Schouten [19] at higher pressures. The experimental investigations agreed on the position of the critical line and the three-phase line solid–fluid–fluid, but not on the shapes of the fluid–fluid equilibrium curve and the liquidus of the hydrogen-rich solid–fluid (SF) equilibrium. Loubeyre *et al* found a cusp on the helium-rich side of the fluid–fluid curve and also found that the liquidus of the SF equilibrium is nearly pressure independent up to 35 mole percent helium, before it rises to the three-phase equilibrium. Van den Bergh and Schouten observed a smooth fluid–fluid surface and a nearly linear increase of the liquidus of the SF equilibrium to the three-phase line. Furthermore, density inversion was observed, i.e. the solid phase has a smaller mass density than the hydrogen-rich fluid phase. Theoretical calculations using variational theory combined with the VDW1F approximation were performed by Ree [2] and van den Bergh and Schouten [3]. Both theoretical investigations yield a phase diagram in quantitative accordance with the experiments of [19], except for the width of the fluid–fluid coexistence curves. One of the aims of this paper is to see whether the HMSA integral equations (a hybrid combination of the hypernetted chain closure and the mean spherical approximation) yield an improved result.

An important point that was not addressed in either theoretical or experimental investigations is the solubility in the solid phases. This phenomenon can affect the metallization of hydrogen and therefore also influence the properties of the solid cores of Saturn and Jupiter. The occurrence of solubility in a solid phase at high pressure has

Table 1. The exponential-6 parameters of helium–hydrogen taken from [3], [21] and [22].

	α_{ij}	ε_{ij}/k_B (K)	r_{ij}^* (Å)
He–He	13.1	10.8	2.9673
H_2–H_2	11.1	36.4	3.43
He–H_2	12.49	17.3	3.28

been demonstrated recently in the related system He–N_2 by Vos and Schouten [20]. The system He–H_2 was chosen for the present study to investigate a possible solubility of helium in the hydrogen-rich solid.

In summary, it is the purpose of the present paper to test the use of integral equations and DFTF on binary mixtures at high pressure, to calculate the fluid–fluid phase separation from integral equations, to investigate possible solubility in the solid phase of hydrogen and to address the difference between the experimental findings on He–H_2. In section 2, the integral equations are outlined and compared with computer simulations and the potential models are defined. The fluid–fluid separation is treated in section 3. The DFTF is outlined and applied in section 4 and a summary and conclusions are presented in section 5.

2. Interaction potentials and fluid structure

The exponential-6 pair potential is known to describe the interactions of molecular substances well over a large range in density at high pressure. It has the following form:

$$\varphi_{ij}(r) = \frac{\varepsilon_{ij}}{\alpha_{ij} - 6}\left\{6\exp\left[\alpha_{ij}\left(1 - \frac{r}{r_{ij}^*}\right)\right] - \alpha_{ij}\left(\frac{r_{ij}^*}{r}\right)^6\right\} \tag{1}$$

where ε_{ij} is the well depth, r_{ij}^* is the separation at the minimum of the well and α_{ij} is a parameter that varies the stiffness of the repulsion. The parameters for helium were fitted by Young *et al* [21] to the melting line and the equation of state (EOS) up to 120 kbar. The hydrogen potential was fitted by Ross *et al* [22] to beam scattering data, *ab initio* calculations and shock-wave data. The unlike interaction was fitted by van den Bergh and Schouten [3] to the experimental binodal curve over a large pressure range using variational theory. The values of the parameters are given in table 1.

At present, the use of integral equations is a well established method for computing the structure and the EOS of a pure fluid [5–8]. In brief, one must simultaneously solve the Ornstein–Zernike relation and an additional closure relation between the radial distribution function $g(r)$, the direct correlation function $c(r)$ of the fluid and the interaction potential $\varphi(r)$ [23].

For He–H_2, the HMSA closure of Zerah and Hansen [6] seems very suitable, since it is a self-consistent closure and its results compare well with simulation data [5, 6]. Here, self-consistency means that the compressibility χ_T obtained through the virial expression is consistent with the compressibility calculated from the structure factor $S(k)$ at $k = 0$ (fluctuation compressibility). The resulting integral equations are readily solved according to the iteration scheme of Gillan [24]. The difference between the fluctuation compressibility and the virial compressibility was kept smaller than 3 parts in 1000. This is a trade-off between accuracy and computing time.

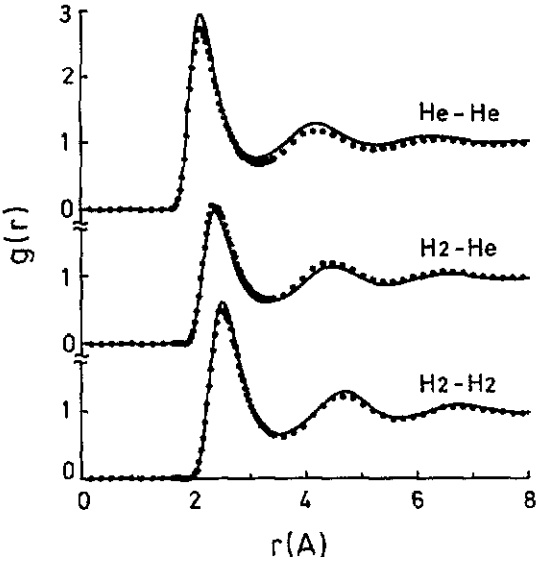

Figure 1. Radial distribution functions of a mixture containing 50 mole percent hydrogen at 300 K and 7.0 $cm^3\ mol^{-1}$. The dots represent the results from the MC simulations and the drawn curves are the results of the HMSA integral equation.

Table 2. Comparison of pressures of the binary mixture helium–hydrogen calculated from two-component Monte Carlo simulations and the HMSA integral equation. Numbers in parentheses denote variation in the last digit.

			$P_{classical}$ (kbar)	
T (K)	x_{H_2}	V (cc/mole)	MC	HMSA
100	0.10	8.5	9.82(3)	9.67
100	0.80	10.8	11.28(6)	11.37
300	0.00	4.7	86.2(8)	87.9
300	0.25	7.0	37.9(2)	37.8
300	0.50	7.0	53.7(1)	53.2
300	1.00	8.8	41.5(3)	41.4

In order to check the solutions of the integral equation, we compare the radial distribution functions (RDF) and pressures with simulation results. Two-component (NVT) Monte Carlo simulations were performed on 500 particles interacting through the potential of (1) with the parameters of table 1 at 100 K on 10 mole percent hydrogen in helium at a volume of 8.5 $cm^3\ mol^{-1}$ (10 kbar) and on 80 mole percent hydrogen in helium at 10.8 $cm^3\ mol^{-1}$ (11 kbar). At 300 K, simulations were performed on pure helium at 4.7 $cm^3\ mol^{-1}$ (86 kbar), 25 mole percent hydrogen in helium at 7.0 $cm^3\ mol^{-1}$ (38 kbar), 50 mole percent hydrogen in helium at 7.0 $cm^3\ mol^{-1}$ (54 kbar) and pure hydrogen at 8.8 $cm^3\ mol^{-1}$ (42 kbar). We used 2×10^5 configurations for equilibration and 2×10^5 configurations for production. Since it is known that the HMSA integral equation works very well for pure substances [5, 6], it is interesting to compare the RDF of the 50 mole percent hydrogen mixture. It can be seen from figure 1 that the agreement is good. The RDF of the like species are systematically a little higher than the simulation results while the RDF of the unlike species is somewhat lower. The comparison of the pressures is shown in table 2. The present comparisons form a severe test, since the

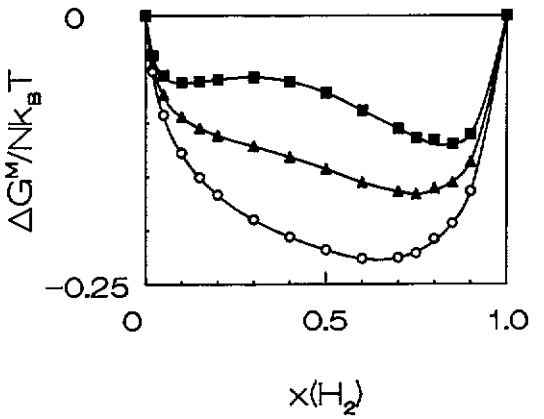

Figure 2. The free enthalpy on mixing versus composition at 300 K. ○, the results at 40 kbar; ▲, at 50 kbar and ■, at 60 kbar.

conditions are either close to the binodal curve or close to the melting line. It can be seen from table 2 that the agreement in pressure is very good, ranging from −2 to +2%. Therefore, we conclude that the HMSA integral equations are useful to calculate both the structure and thermodynamics of binary mixtures at high density.

3. Fluid–fluid separation: the binodal and spinodal curves

We have calculated the compressibility factor $\beta p/\rho$ of the homogeneous fluid including the Wigner–Kirkwood quantum correction as a function of density for 14 compositions at 100 K and 16 compositions at 300 K [25]. For each composition, typically 25–40 points were used to fit the data to a polynomial of the sixth degree. The standard deviations of the fits varied between 5×10^{-4} and 5×10^{-3}. These isotherms were integrated with respect to density. The ideal contribution $\log(\rho)$ and the entropy of mixing were added to obtain the Helmholtz free energy F:

$$F(T,\rho,x) = Nk_BT\left(\int_0^\rho \frac{p(\rho') - p_{id}(\rho')}{\rho'^2}\,d\rho' + \log(\rho) + \sum_i x_i \log(x_i) + C\right) \qquad (2)$$

where ρ is the density, p the pressure, p_{id} is the pressure of the ideal gas and x_i the mole fraction of species i. In order to obtain the Gibbs free enthalpy G at constant pressure, F was calculated at that particular pressure and the pV term was added. The free enthalpy of mixing ΔG^m is obtained from:

$$\Delta G^m(T,p,x) = G(T,p,x) - xG(T,p,1) - (1-x)G(T,p,0). \qquad (3)$$

We constructed the double tangent to obtain the compositions of the coexisting phases. Examples of $\Delta G^m(p,x)$ at three different pressures as a function of the hydrogen composition are shown in figure 2. At 100 K, the isotherms had to be extrapolated over a factor of two in pressure from the broken curve in figure 3 at the intermediate compositions ($0.2 < x_{H_2} < 0.7$), since no solutions of the HMSA equations could be obtained (see below). This extrapolation yielded scatter in the ΔG^m data in this concentration range. Therefore, the demixing could only be calculated for pressures above

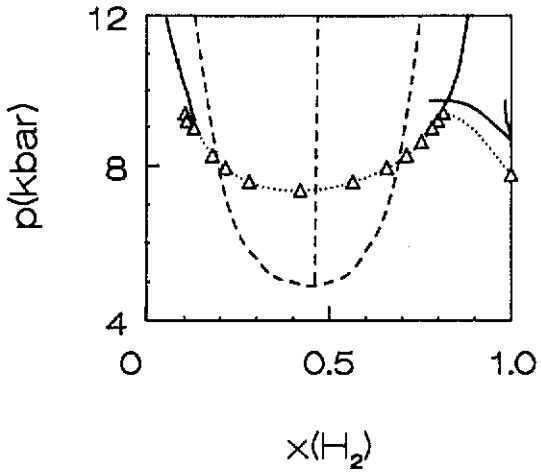

Figure 3. The phase diagram at 100 K. △ and the dotted curve are the experimental binodal curve of Streett [17] and melting point of Mills *et al* [37]. The full curves are the calculated fluid–fluid binodal curve, the liquidus and the solidus. The broken curve is the calculated spinodal curve and the broken line is the rectilinear diameter.

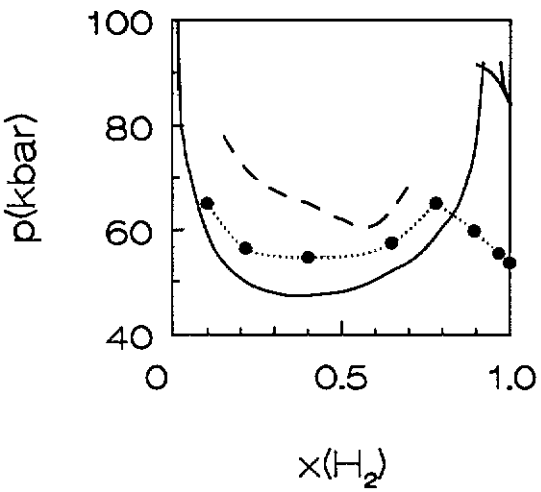

Figure 4. The phase diagram at 300 K. The dots and the broken curve are the binodal curve and liquidus of van den Bergh and Schouten [19] and Diatschenko *et al* [39]. The full curves are the calculated fluid–fluid binodal curve, the liquidus and the solidus. The broken curve is the calculated spinodal curve.

9 kbar. At 300 K, no extrapolation was needed. Close to the critical point, it becomes difficult to construct a double tangent due to the flatness of the ΔG^m curve. The critical composition was determined from the intersection of short extrapolations of the rectilinear diameter [26] and the binodal curve. From figure 3, it can be seen that at 100 K, the resulting binodal curve is in good agreement with the experimental data of Streett [17]. The critical composition is about 46 mole percent hydrogen at the experimental critical pressure, in reasonable agreement with the experimental value of 42%. The results at 300 K are shown in figure 4, together with the experimental results of van den Bergh and Schouten [19]. It can be seen that the calculated binodal curve is lower than the experimental one by about 7 kbar. This difference is nearly constant over a large composition interval. This indicates that the width of the calculated binodal curve is the same as that found in the experiment [19], while this was a problem with perturbation theory [3]. The calculated critical composition of 38 mole percent hydrogen is in reasonable agreement with the experimentally determined value of 42%. Note that the calculated binodal curve does not show a cusp as was reported by Loubeyre *et al* [18].

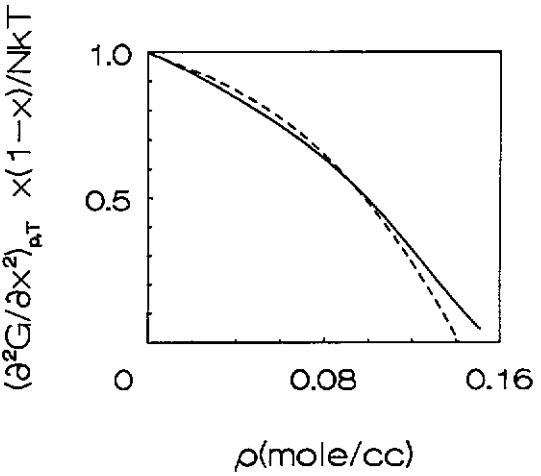

Figure 5. The second derivative of the free enthalpy with concentration $(\partial^2 G/\partial x^2)_{p,T}$ reduced with $x(1-x)/Nk_BT$ versus density at 300 K and a composition of 40 mole percent hydrogen. The full line is the result calculated from the Bhatia–Thornton structure factor and the broken line is the result from the ΔG^m (3).

In [3], the parameters of the unlike interaction were adjusted to get agreement with the experimental data. Also, in this case the agreement can be improved by slightly varying the unlike interaction. However, the interaction of pure hydrogen [22] also deserves attention, since at 100 K the differences in pressure with the experimental EOS of Mills *et al* [27] is about 30% at 2 kbar and about 15% near the melting line. At 300 K and 2 kbar, the difference with Mills *et al* was about 18%. This is outside the combined errors of the HMSA equation (see the previous section) and Mills *et al*.

Bhatia and Thornton [28] have constructed three structure factors for binary mixtures from the Fourier transforms of the local number density $N(k)$ and the composition $C(k)$. The composition fluctuations are represented by the structure factor $S_{CC}(k)$, defined as:

$$S_{CC}(k) = N \cdot \langle C^*(k) \cdot C(k) \rangle \tag{4}$$

where the brackets denote ensemble average. From this structure factor, it is possible to calculate the second derivative of the free enthalpy with respect to composition, $(\partial^2 G/\partial x^2)_{p,T}$, at constant pressure and temperature, since:

$$\left(\frac{\partial^2 G}{\partial x^2}\right)_{p,T} = \lim_{k \to 0} \frac{Nk_B T}{S_{CC}(k)}. \tag{5}$$

It is convenient to scale this expression with the product of the mole fractions of both components, since in the limit of zero density, $S_{CC}(0)$ is equal to $x(1-x)$. Setting this second derivative equal to zero determines the spinodal curve, i.e. the curve where a (meta)stable mixture becomes unstable with respect to composition fluctuations. The spinodal curve always lies inside the binodal, except in the critical point, where both curves touch. Since the integral equation does not yield an accurate solution near the spinodal curve, $(\partial^2 G/\partial x^2)_{p,T}$ has to be extrapolated as a function of density or pressure to find the zero crossing. An example of $(\partial^2 G/\partial x^2)_{p,T}/Nk_BT$, normalized with the mole fractions, as a function of density at $x_{H_2} = 40\%$ and $T = 300$ K is shown in figure 5. With increasing density, it decreases from its limiting value 1, steepening with increasing density. At high density, however, an inflection point occurs. On some occasions (100 K and 60%), even two inflection points showed up. We had no reason to expect inflection points, since from figure 2, it can be seen that the bump on the ΔG^m curves increases monotonously with pressure. For comparison, we have calculated

$(\partial^2 G/\partial x^2)_{p,T}/Nk_BT$ directly from $\Delta G^m(x)$, in fitting $G^{exc} = \Delta G^m - \Sigma_i x_i \log(x_i)$ as a function of mole fraction with a polynomial [29]. Using this method, we found no inflection points on $(\partial^2 G/\partial x^2)_{p,T}/Nk_BT$ as a function of density and also, the density of the zero crossing was lower. Furthermore, we have calculated $(\partial^2 G/\partial x^2)_{p,T}$ as a function of density for a system interacting through a $(1/r)^{12}$ potential with parameters mimicking [30] He–H_2. Again, we found no inflection points. We used a short linear extrapolation to determine the density at the zero crossing of $(\partial^2 G/\partial x^2)_{p,T}/Nk_BT$ calculated from $S_{CC}(0)$. The spinodal curve thus obtained for $T = 100$ K is also shown in figure 3. It is clear that the spinodal and binodal curves do not touch in the critical point and that the spinodal curve does not lie completely inside the binodal curve. At $T = 300$ K, the spinodal curve does lie inside the binodal curve, but is is about 17 kbar higher than the calculated binodal curve at the critical composition, see figure 4.

We have checked whether this inconsistency might be due to round-off errors in the Gillan [24] iteration scheme. For this reason, different mesh sizes were used, but no noticeable difference was found. A reason why $(\partial^2 G/\partial x^2)_{p,T}$ may come out wrong at high density is that self-consistency of the compressibility χ_T, does not necessarily mean consistency of $(\partial^2 G/\partial x^2)_{p,T}$. Since we are in fact dealing with two densities (of the different species), one should in principle take two consistency criteria.

Note that the discrepancies between the spinodal and binodal cruves bear resemblance with the recent results of Lomba [31] for a system of pure Lennard–Jones molecules with the self-consistent RHNC closure. Lomba also finds a region where the binodal curve cannot be calculated through integral equations. Furthermore, it has also been found that the Born–Green integral equation has problems near the critical point of a square well system [32]. On the other hand, at 300 K we find that one can obtain solutions of the HMSA integral equations beyond the critical point.

Nevertheless, since the binodal curves are calculated from isotherms that are in very good agreement with computer simulations (cf section 2), we believe that they are reliable and it is the spinodal curve that needs improvement. The fact that the binodal curves calculated from the HMSA integral equation are in reasonable agreement with experiments at very high pressure indicate the power of this integral equation.

4. Solid–fluid equilibria

In a previous paper [16], we showed that using the Haymet and Oxtoby [33] (HO) formulation of DFTF and discarding the first reciprocal lattice vector (RLV) where the direct correlation function is negative, as proposed by Rovere and Tosi [34], reasonable agreement with experiments on pure helium and hydrogen could be obtained. In the HO formulation, the grand potential Ω_S of a solid phase is expanded around the grand potential Ω_F of the coexisting fluid, while assuming constant chemical potential μ, volume V and temperature T. For binary mixtures, this expansion reads [12]:

$$\frac{\beta(\Omega_S - \Omega_F)}{N} = \sum_{i=1}^{2} \int d\boldsymbol{r}\left(\rho_i(\boldsymbol{r}) \log\left(\frac{\rho_i(\boldsymbol{r})}{\rho_{iF}}\right) - (\rho_i(\boldsymbol{r}) - \rho_{iF})\right)$$
$$- \tfrac{1}{2} \sum_{i,j=1}^{2} \int\int d\boldsymbol{r}\, d\boldsymbol{r}'\, c_{ij}(|\boldsymbol{r} - \boldsymbol{r}'|)(\rho_i(\boldsymbol{r}) - \rho_{iF})$$
$$\times (\rho_j(\boldsymbol{r}) - \rho_{jF}) + \text{higher-order terms} \qquad (6)$$

Table 3. Comparison of the experimental [17, 19] and calculated freezing pressures and transition volumes of the mixture helium–hydrogen and comparison of the calculated fluid and solid mass densities. The compositions of the solid and the mass densities are calculated quantities.

$T = 100$ K

x_{H_2}		p (kbar)		V_{fluid} (cc/mole)		V_{solid} (cc/mole)		ρ (g/cc)	
fluid	solid	expt.	calc.	expt.	calc.	expt.	calc.	fluid	solid
0.00	0.00	21.77	21.17	6.65	6.68	6.45	6.15		
0.02	0.00	—	20.77	—	6.81	—	6.16		
0.80	0.983	—	9.70	—	11.78	—	11.43	0.204	0.178
0.90	0.984	—	9.49	—	12.19	—	11.41	0.180	0.178
1.00	1.00	7.77	8.66	13.75	12.79	13.18	11.70	0.156	0.171

$T = 300$ K

x_{H_2}		p (kbar)		V_{fluid} (cc/mole)		V_{solid} (cc/mole)		ρ (g/cc)	
fluid	solid	expt.	calc.	expt.	calc.	expt.	calc.	fluid	solid
0.00	0.00	121.0	134.6	4.4	4.19	4.3	3.95		
0.02	0.00	—	130.4	—	4.29	—	3.95		
0.90	0.972	59.5	91.6	—	6.87	—	6.67	0.320	0.308
0.95	0.976	56.8	89.6	—	7.01	—	6.72	0.300	0.305
1.00	1.00	53.7	84.1	8.2	7.23	8.0	6.90	0.277	0.290

where $\beta = 1/k_B T$, $\rho_i(\boldsymbol{r})$ is the solid density of component i, ρ_{iF} is the fluid density of component i and $c_{ij}(|\boldsymbol{r} - \boldsymbol{r}'|)$ is the fluid direct correlation function between species i and j at densities ρ_{iF} and ρ_{jF}. This series is usually truncated after second order for lack of information on the higher-order correlation functions. The solid density is conveniently parametrized as a sum of Gaussians on an HCP lattice. In reciprocal space this reads:

$$\rho_i(\boldsymbol{r}) = \rho_{iS} \sum_{G} e^{-G^2/4\alpha_i} e^{iG\cdot r} \tag{7}$$

where G denotes the RLV, ρ_{iS} is the average solid density and α_i is the inverse width squared of the Gaussian peaks of component i. Equation (6) is minimized with respect to α_i and ρ_{iS} at constant fluid density, since at equilibrium, Ω equals the grand potential and thus, $\Omega = -pV$. The freezing point is obtained by varying ρ_{iF} until $\Omega_S = \Omega_F$, which implies equal pressures of both phases. In practice, the density was varied at constant composition of the fluid phase to yield the freezing point. The fluid direct correlation functions were calculated with the HMSA integral equations. This is a good description of the fluid structure. For the crystal structure, we took the HCP lattice, since it is experimentally determined that this is the structure of the solid that coexists with the fluid for hydrogen [35] and for helium (see [36] and references therein). In order to obtain agreement with the experiments, the fourth RLV was omitted [16, 34] from the sum in (7). For the HCP lattice, this vector corresponds to negative values of $\hat{c}(\boldsymbol{k})$, so that the fluid phase is stabilized ($\hat{c}(\boldsymbol{k})$ is the Fourier transform of the direct correlation

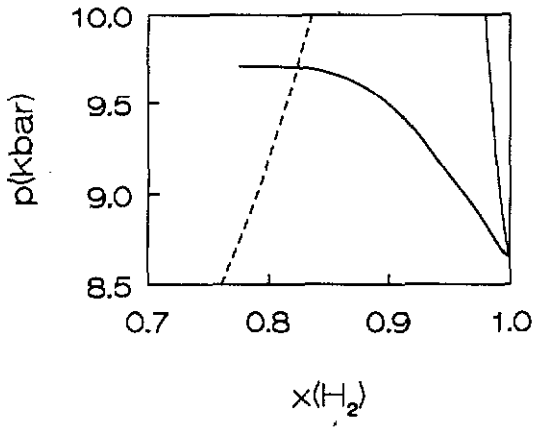

Figure 6. The solid–fluid equilibrium at 100 K calculated with DFTF. The full curves are the liquidus and the solidus. The broken curve is the calculated fluid–fluid binodal curve.

Table 4. Comparison of the calculated three-phase equilibria with the experimental results of [17] and [19]. F1 denotes the helium-rich fluid, F2 the hydrogen-rich fluid and S the hydrogen-rich solid. Compositions are in mole fraction hydrogen.

	p (kbar)		x_{F1}		x_{F2}		x_S	
T (K)	expt.	calc.	expt.	calc.	expt.	calc.	expt.	calc.
100	9.35	9.7	0.104	0.115	0.813	0.82	—	0.983
300	64.7	91	0.11	0.02	0.78	0.92	—	0.97

function). The sum was carried out over 1800 reciprocal lattice vectors to achieve convergence.

The results for the freezing at 100 K at the hydrogen-rich side are shown in figures 3 and 6 (detail) and table 3. The pressure of the liquidus increases smoothly with decreasing mole fraction H_2. The solidus increases steeply with mole fraction H_2, the solubility being 1.7 mole percent helium at the highest calculated state point. The agreement with the freezing point of pure hydrogen [37] and the three-phase line solid–fluid–fluid [17] (see table 4) is good. However, this good agreement is due to a fortuitous cancellation of errors, since for pure hydrogen, the calculated volume of the fluid at the transition is 10% smaller than the experimental value [27]. This is partly compensated because the calculated isotherm is 15% off in pressure in this region. An interesting point is shown in table 3: for the compositions 0.8 and 0.9, the fluid has a higher mass density than the solid. This results in density inversion of the solid and fluid phases, that has also been observed experimentally [19]. For pure helium, the freezing pressure is in good agreement with the experimental data [38] (see table 3). For a fluid mixture with 2% hydrogen, there is no solubility of hydrogen in the solid. Note however, that the phase separation is found at pressures lower than the melting point of helium. This means that *below* the freezing pressure of helium, a solid consisting of pure helium grows from a helium-rich fluid mixture, while starting from a pure helium fluid, no solid would yet grow. This is of course inconsistent. If a helium-rich mixture freezes at a lower pressure than the pure component, there should be a peritectic point and thus a solubility in the solid that is larger than in the fluid. We have checked this by constraining the solid

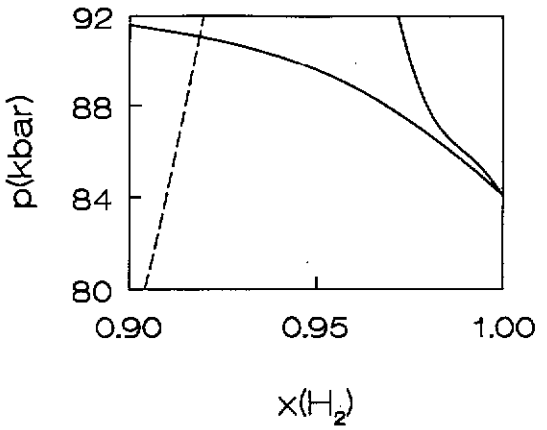

Figure 7. The solid–fluid equilibrium at 300 K calculated with DFTF. The full curves are the liquidus and the solidus. The broken curve is the calculated fluid–fluid binodal curve.

composition to be higher than the fluid composition. As a result, no minimum of Ω_S as a function of ρ_{iS} occurred.

At 300 K (see figures 4 and 7 and table 3), the pressure of the liquidus also increases gradually from the freezing point of hydrogen, in agreement with the results of Schouten and van den Bergh [19]. The solubility of helium in the solid is about 3 mole percent at the pressure of the three-phase equilibrium. However, the quantitative agreement with experiments [19, 39] is bad, since the transition pressure found is 60% too high. As a result, the agreement of the calculated three-phase line with the experimental one is also bad, see table 4. It can be seen from table 3 that density inversion occurs for a fluid containing 10% helium, but not for 5% helium and smaller mole fractions. This is in reasonable agreement with experiments [19], where at most 6% was needed to obtain density inversion. On the helium-rich side, the agreement of the calculated freezing pressure with experiment [38] is remarkable, see table 3. However, the same inconsistency occurs as at 100 K. Again, the helium-rich fluid is found to be in equilibrium with a pure helium solid at pressures *below* the freezing pressure of pure helium.

We can think of three possible reasons for this inconsistency. Firstly, it may be due to the omission of the fourth RLV of the HCP lattice. We have performed calculations at 100 K taking into account the fourth RLV. Pure helium then freezes at 75 kbar into an HCP lattice, while a mixture with 2% hydrogen freezes at 62 kbar into a solid consisting of pure helium. These results have to be considered with care, since we had to extrapolate Ω_S–Ω_F to obtain the transition points. Nevertheless, it suggests that the omission of the fourth star of the HCP lattice is not the cause of the inconsistency.

Secondly, the helium-rich fluid may be metastable with respect to demixing into a hydrogen-rich solid and a helium-rich fluid ($S_{H_2}F$). We found that at $T = 300$ K and at the freezing pressure of helium a mixture containing 2% hydrogen was indeed metastable with respect to fluid–fluid separation and thus certainly to demixing into a fluid and a hydrogen-rich solid. It is then likely that the solidus and liquidus that start from the helium melting point do increase and cross the $S_{H_2}F$ equilibrium at a very small mole fraction hydrogen. Thus, at 2% hydrogen, one should obtain coexistence with a hydrogen-rich solid. We have tried to obtain such a coexistence but did not find one, probably because the difference in density is too large (about 50%) and the difference in concentration is also very large (the concentration of the solid is about 97% and of the fluid less than 2%), causing the expansion to break down.

In the third place, the inconsistency may be due to the truncation of the expansion of the grand potential of the solid (7) after second order. Unfortunately, it is not possible to calculate the three-particle direct correlation function for a mixture at these high densities. On the other hand, in the phase diagram calculated for a mixture of Lennard–Jones molecules with a diameter ratio of 0.9 by the same expansion (see [14], figure 8), an analogous inconsistency occurs. In this case, an azeotropic phase diagram is obtained where, for a mole fraction of the large molecules above 0.5, the solidus is at higher temperatures than the liquidus.

5. Summary and conclusions

The self-consistent HMSA integral equation has been tested on the system helium–hydrogen at very high density. The results for the pressure and the radial distribution functions are in good agreement with computer simulations. From the resulting isotherms, the fluid–fluid demixing was calculated. It is in fair agreement with the experimental results of Streett and van den Bergh and Schouten. This demonstrates the usefulness of the HMSA integral equation for binary mixtures and the consistency of the HMSA results with variational perturbation theory with which the unlike interaction was determined. The width of the binodal curve is in far better agreement with experiments than the one calculated from variational theory with the VDWIF approximation. Therefore, it seems worthwhile to tune the unlike interaction potentials with the help of the HMSA integral equation to the experimental results. The spinodal curve, calculated from the composition fluctuation structure factor $S_{CC}(k)$ is not consistent with the calculated binodal curve. The reason for this inconsistency is probably that the self-consistency of the integral equations is not imposed on $S_{CC}(k)$.

The solid–fluid equilibria of the mixture were calculated using the density functional theory of freezing in the formulation of Haymet and Oxtoby, truncating the expansion after second order and leaving out the fourth RLV. At 100 K, the agreement with experiments is good at the hydrogen-rich side, but this is probably fortuitous. At 300 K, on the hydrogen-rich side, the shape of the liquidus is in agreement with the experimental result of van den Bergh and Schouten. The agreement with the experiments is qualitative. On both isotherms, we find a solubility of helium in the hydrogen-rich solid of a few percent. It is interesting to verify this result experimentally. The unusual phenomenon of density inversion between the solid and fluid phases is found, in agreement with experiments. For pure helium, the agreement with experimental data is good. In contrast, a mixture containing mostly helium is found to freeze into a pure helium solid at a pressure *below* the freezing pressure of pure helium, which is inconsistent. Probably, such a mixture should freeze into a hydrogen-rich solid that has a very different density, so that the expansion breaks down. Therefore, the present version of DFTF seems useful as long as the difference in density between the coexisting phases is not too large.

Acknowledgments

We thank Jean-Pierre Hansen for useful discussions. WLV and AdK wish to thank the colleagues at the ENSL for a very enjoyable stay. This work has been financially supported by the Centre National de Recherche Scientifique (CNRS, France) and the Netherlands Organisation for Scientific Research (NWO, the Netherlands).

References

[1] Schouten J A 1989 *Phys. Rep.* **172** 33
[2] Ree F H 1983 *J. Phys. Chem.* **87** 2846
[3] van den Bergh L C and Schouten J A 1988 *J. Chem. Phys.* **89** 2236
[4] Ree F H 1983 *J. Chem. Phys.* **78** 409
[5] Talbot J, Lebowitz J L, Waisman E M, Levesque D and Weis J-J 1986 *J. Chem. Phys.* **85** 2187
[6] Zerah G and Hansen J-P 1986 *J. Chem. Phys.* **84** 2336
[7] Rodgers F J and Young D A 1984 *Phys. Rev.* A **30** 999
[8] Lado F, Foiles S M and Ashcroft N W 1983 *Phys. Rev.* A **28** 2374
[9] Haymet A D J 1987 *Ann. Rev. Phys. Chem.* **38** 98
Baus M 1990 *J. Phys.: Condens. Matter* **2** 2111
[10] Lutsko J F and Baus M 1990 *Phys. Rev. Lett.* **64** 761
[11] Barrat J-L, Baus M and Hansen J-P 1987 *Phys. Rev. Lett.* **56** 1063; 1987 *J. Phys. C: Solid State Phys.* **20** 1413
[12] Smithline S J and Haymet A D J 1987 *J. Chem. Phys.* **86** 6486; 1988 Erratum **88** 4104
[13] Zeng X C and Oxtoby D W 1990 *J. Chem. Phys.* **93** 4357
[14] Rick S W and Haymet A D J 1989 *J. Chem. Phys.* **90** 1188
[15] Kranendonk W G T and Frenkel D 1989 *J. Phys.: Condens. Matter.* **1** 7735
[16] de Kuijper A, Vos W L, Barrat J-L, Hansen J-P and Schouten J A 1990 *J. Chem. Phys.* **93** 5187
[17] Streett W B 1973 *Astrophys. J.* **186** 1107
[18] Loubeyre P, LeToullec R and Pinceaux J-P 1985 *Phys. Rev.* B **32** 7611; 1987 **36** 3732
[19] Schouten J A, van den Bergh L C and Trappeniers N J 1985 *Chem. Phys. Lett.* **114** 410; 1986 *Fluid Phase Eq.* **32** 1
van den Bergh L C, Schouten J A and Trappeniers N J 1987 *Physica* **141A** 524
[20] Vos W L and Schouten J A 1990 *Phys. Rev. Lett.* **64** 898
[21] Young D A, McMahan A K and Ross M 1981 *Phys. Rev.* B **24** 5119
[22] Ross M, Ree F H and Young D A 1983 *J. Chem. Phys.* **79** 1487
[23] Hansen J-P and McDonald I R 1986 *Theory of Simple Liquids*, 2nd edn (London: Academic)
[24] Gillan M J 1979 *Mol. Phys.* **38** 1781
[25] The compositions are 0.00, 0.05, 0.10, 0.15, 0.20, 0.30, 0.40, 0.50, 0.60, 0.70, 0.80, 0.90, 0.95 and 1.00 given in mole fraction hydrogen. At 300 K, we also included 0.02, 0.75 and 0.85 and omitted 0.95
[26] The rectilinear diameter is the mean of the two branches of the fluid–fluid separation curve.
[27] Mills R L, Liebenberg D H, Bronson J C and Schmidt L C 1977 *J. Chem. Phys.* **66** 3076
[28] Bhatia A B and Thornton D E 1970 *Phys. Rev.* B **2** 3004
[29] G^{exc} is more conveniently fitted by a polynomial.
[30] Schouten J A, Sun T F and de Kuijper A 1990 *Physica* **169A** 17
[31] Lomba E 1989 *Mol. Phys.* **68** 87
[32] Fisher M E and Fishman S 1981 *Phys. Rev. Lett.* **47** 421
[33] Haymet A D J and Oxtoby D W 1981 *J. Chem. Phys.* **74** 2559
[34] Rovere M and Tosi M P 1985 *J. Phys. C: Solid State Phys.* **18** 3445
[35] Hazen R M, Mao H K, Finger L W and Hemley R J 1987 *Phys. Rev.* B **36** 3944
[36] Vos W L, van Hinsberg M G E and Schouten J A 1990 *Phys. Rev.* B **42** 6106
[37] Mills R L, Liebenberg D H and Bronson J C 1978 *Phys. Rev.* B **18** 4526
[38] Mills R L, Liebenberg D H and Bronson J C 1980 *Phys. Rev.* B **21** 5137
[39] Diatschenko V, Chu C W, Liebenberg D H, Young D A, Ross M and Mills R L 1985 *Phys. Rev.* B **32** 381